Infinite, undulating chains of intermolecularly hydrogen bonded (*E*,*E*)-2,2-dimethylcyclohexane-1,3-dione dioximes in the solid state. A single crystal X-ray, charge density distribution and spectroscopic study

Albert W. Marsman,[a] Cornelis A. van Walree,[a] Remco W. A. Havenith,[ab] Leonardus W. Jenneskens,[a]* Martin Lutz,[c] Anthony L. Spek,[c] Egbertus T. G. Lutz[d]† and Joop H. van der Maas[d]

[a] *Debye Institute, Department of Physical Organic Chemistry, Utrecht University, Padualaan 8, 3584 CH Utrecht, The Netherlands. E-mail: jennesk@chem.uu.nl; Tel.: +31 302533128, Fax.: +31 302534533*
[b] *Debye Institute, Theoretical Chemistry Group, Utrecht University, Padualaan 8, 3584 CH Utrecht, The Netherlands*
[c] *Bijvoet Center for Biomolecular Research, Crystal and Structural Chemistry, Utrecht University, Padualaan 8, 3584 CH Utrecht, The Netherlands*
[d] *Department of Vibrational Spectroscopy, Utrecht University, Sorbonnelaan 16, 3584 CA Utrecht, The Netherlands*

Received (in Cambridge, UK) 18th October 1999, Accepted 10th December 1999

In the solid state (*E*,*E*)-2,2-dimethylcyclohexane-1,3-dione dioxime (**1**) and (*E*,*E*)-2,2,5,5-tetramethylcyclohexane-1,3-dione dioxime (**2**) give infinite, undulating polymer-like chains due to intermolecular dimeric oxime hydrogen bonding [$R_2^2(6)$ motif with C_i-symmetry; single crystal X-ray analyses]. Configurational stereoisomerism of the oxime groups is prevented by the two methyl groups at the 2-positions. Consequently, the oxime groups of both **1** and **2** are unequivocally defined and show no disorder. Whereas **1** has molecular C_S-symmetry, compound **2** lacks symmetry and two distinct intermolecular dimeric oxime hydrogen bonds are found.

In the case of **2**, its charge density distribution was determined from high resolution X-ray data and subjected to a Bader type topological analysis giving for the first time insight into the chemical bonding of this dimeric intermolecular oxime hydrogen-bonding motif. The multipole populations and the properties of the (3, −1) bond critical points confirm the lack of symmetry for **2**. All located (3, −1) bond critical points except those of the hydrogen bonds have negative values for the Laplacians $\nabla^2\rho(\boldsymbol{r}_p)$ in line with covalent bonding. Notwithstanding, the description of the two distinct O–N bonds of **2** is not fully adequate; to obtain negative Laplacian values at their bond critical points, hexadecapole parameters ($l = 4$) for C, N and O had to be used in the refinement. By comparison with B3LYP/6-311++G** results on acetone oxime it is shown that this anomaly can be attributed to deviations in the experimentally determined charge density distribution of the two distinct O–N bonds of **2**. The positive Laplacians for the hydrogen bonds agree with closed shell interactions.

In addition, the spectroscopic properties of the intermolecular oxime hydrogen bonding $R_2^2(6)$ motifs of **1** and **2** were studied using ^{13}C CP/MAS NMR and IR and Raman spectroscopy. ^{13}C CP/MAS NMR showed that for **1** and **2** one and two distinct oxime hydrogen bonding motifs, respectively, are discernible. From their IR and Raman spectra unequivocal proof was obtained that the $R_2^2(6)$ motifs possess local C_i-symmetry.

Introduction

Directional intermolecular hydrogen bonds represent an important motif for (self)-assembly of molecular building blocks into supramolecular materials.[1] Although various functionalities have been applied,[2] the oxime functionality [–C(R)=NOH] has been largely neglected. This is surprising since a survey of single crystal X-ray structural data of 231 oxime derivatives[3] (Cambridge Crystallographic Database) revealed that 54% participate in (self)-complementary intermolecular dimeric oxime hydrogen bonding [graph-set notation: $R_2^2(6)$ motif].[2] Hence, this motif may be useful in supramolecular chemistry.[2] Previously, we studied the assembly of semi-rigid rodlike oligo(cyclohexylidenes)‡ and their saturated analogues bearing either one or two oxime end groups in the solid state.[4,5] Whereas for all mono-oximes linear, centrosymmetric dimers were found,[5a,b] the related dioximes gave infinite linear non-covalent polymer-like chains.[5c,d] A similar oxime hydrogen bonding motif was used by others for the preparation of metal-containing hydrogen-bonded architectures consisting of various pyridine–oxime ligands and Ag^+-ions.[6]

It should be emphasised that due to the high activation barrier for nitrogen inversion in oximes ($\Delta H^{\ddagger}$ 40–50 kcal mol^{-1}) configurational stereoisomerism can occur.[7] § In the case of oligo(cyclohexylidene) mono- and dioximes the presence of two and three stereoisomers, respectively, is responsible for the occurrence of disorder in the oxime groups in the solid state.[5] This disorder has hitherto hindered a detailed analysis of the intermolecular dimeric oxime hydrogen bonding motif. Fortunately, configurational stereoisomerism can be prevented by methyl substitution at one of the α-positions next to an oxime group;[8] due to the steric constraints the oxime group will adopt an *E* configuration.

† Deceased on May 20, 1999.
‡ Oligo(cyclohexylidenes) consist of cyclohexyl-type rings interconnected *via* their 1,4-positions by carbon–carbon double bonds.

§ With respect to the C–C=N plane the OH-group can adopt two positions which are related by a 180° rotation around the C=N bond.

DOI: 10.1039/a908335i

Here we report the solid-state structures of (*E*,*E*)-2,2-dimethylcyclohexane-1,3-dione dioxime (**1**) and (*E*,*E*)-2,2,5,5-tetramethylcyclohexane-1,3-dione dioxime (**2**, Scheme 1). For both compounds *E*/*Z* stereoisomerism of the oxime functionalities is absent. Single crystal X-ray structure analyses show that **1** and **2** assemble into infinite, undulating, polymer-like chains *via* intermolecular dimeric oxime hydrogen bonding [$R_2^2(6)$ motif]; neither **1** nor **2** shows disorder of the oxime groups. The high-resolution X-ray data of **2** allow for the first time an experimental determination of the charge density distribution within this important oxime hydrogen bonding motif; a topological analysis of the charge density distribution in terms of bond-topological parameters was performed.[9] The results are interpreted with the help of B3LYP/6-311++G** data for the model compound acetone oxime. Since in **1** and **2** the intermolecular dimeric oxime hydrogen bonds are unequivocally defined, both compounds were also studied with ^{13}C CP/MAS NMR, IR and Raman spectroscopy.

Results and discussion

Synthesis of 1 and 2

Whereas conversion of cyclohexane-1,3-dione and 5,5-dimethylcyclohexane-1,3-dione into their dioximes gave a mixture of three stereoisomers, respectively [(*E*,*E*, (*E*,*Z*)/(*Z*,*E*) and (*Z*,*Z*), see Scheme 1 and Experimental section],[10–12] conversion of

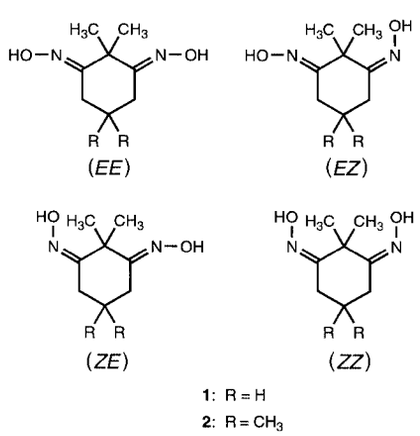

Scheme 1 Possible stereoisomers of **1** and **2**.

either 2,2-dimethyl- or 2,2,5,5-tetramethylcyclohexane-1,3-dione into the dioximes **1** and **2** under similar conditions exclusively gave the (*E*,*E*)-stereoisomers (^1H and ^{13}C NMR). The ketone precursors of **1** and **2** were prepared by methylation of cyclohexane-1,3-dione and 5,5-dimethylcyclohexane-1,3-dione according to a standard procedure (see Experimental section).

Single crystal X-ray structures of 1 and 2

To gain insight in the solid-state topologies of dioximes **1** and **2**, suitable single crystals were grown from saturated acetone solutions by slow evaporation of the solvent and their structures determined by X-ray diffraction. Since the wide angle X-ray diffraction (WAXD) patterns calculated from the single crystal X-ray structure data are identical to the experimentally determined WAXD patterns of native, polycrystalline **1** and **2**, respectively, the X-ray diffraction results are representative for the native compounds (for crystallographic parameters of **1** and **2** see Experimental section). In the single crystal structures of (*E*,*E*)-**1** and (*E*,*E*)-**2** the atom positions of the oxime- (N, O), the methyl groups (C5, C6) as well as C1 are unequivocally defined, *i.e.* oxime disorder is absent! However, in the case of **1** there is a ring puckering disorder concerning the methylene carbon atoms C3/C3a, C3′/C3a′ and C4/C4a (Fig. 1). This

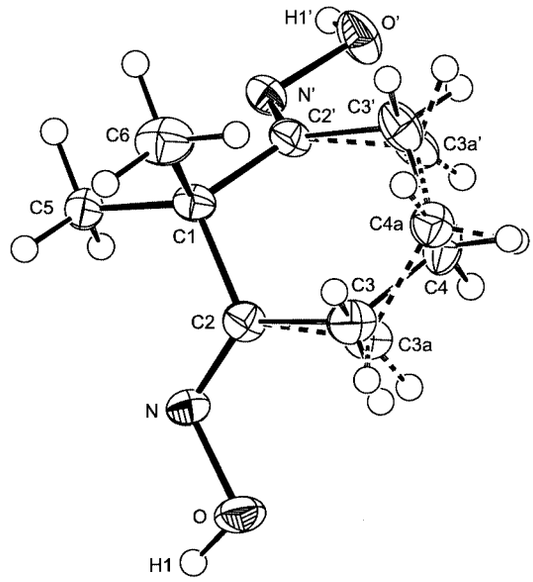

Fig. 1 Displacement ellipsoid plot of **1** (50% probability level). Atoms C3 and C4 are disordered about two positions with an occupation of 65% and 35%. Selected bond lengths, valence- and torsion angles: O–N 1.4146(11) Å, N–C2 1.2718(13) Å, C1–C2 1.5267(13) Å, C2–N–O 113.56(8)°, H1–O–N–C2 −174.8(11)°, (′: x, 0.5 − y, z).

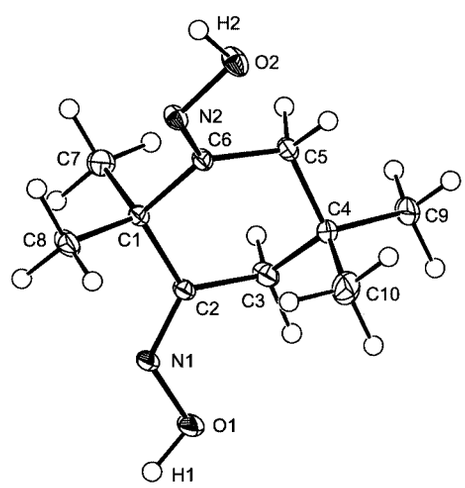

Fig. 2 Displacement ellipsoid plot of **2** (50% probability level, derived from the multipole refinement of high resolution data). Selected bond lengths, valence- and torsion angles: O1–N1 1.4023(5) Å, O2–N2 1.4119(5) Å, N1–C2 1.2827(4) Å, N2–C6 1.2836(4) Å, C1–C2 1.5272(4) Å, C1–C6 1.5315(4) Å, O1–N1–C2 113.89(3)°, O2–N2–C6 113.76(3)°, N1–C2–C1 117.14(3)°, N1–C2–C3 124.52(3)°, C1–C2–C3 118.32(3)°, N2–C6–C1 116.57(3)°, N2–C6–C5 123.68(3)°, C1–C6–C5 119.40(3)°, C1–C2–C3–C4 55.53(4)°, C4–C5–C6–C1 44.55(4)°, H1–O1–N1–C2 177.54°, H2–O2–N2–C6 174.53°.

disorder was resolved in the refined model by splitting the given atoms into two positions. The major (65%) and minor (35%) disorder components correspond to molecules possessing chair- and boat-like conformations, respectively, which due to the *Pnma* space group both possess a mirror plane (molecular C_s-symmetry) containing C1, C4/C4a, C5 and C6. In the case of **2** the disorder in the cyclohexane-like skeleton is absent (Fig. 2).

The oxime groups in **1** and **2** possess *antiperiplanar* conformations and participate in intermolecular dimeric oxime hydrogen bonding.¶ The $R_2^2(6)$ motifs consist of nearly planar six-membered rings (largest deviation from least squares planes: **1**, 0.002 Å; **2**, 0.037 Å and 0.027 Å, respectively) formed by two O–H · · · N hydrogen bonds with crystallographic C_i-symmetry. Whereas for **1** all $R_2^2(6)$ motifs are identical by symmetry, two

¶ *Synperiplanar* oxime groups have never been found in solid-state intermolecular hydrogen bond motifs.

Table 1 Hydrogen bond lengths and angles for **1** and **2**; esd's in parentheses. For atom numbering see Figs. 1 and 2

Compound	Donor–Acceptor	D···A/Å	D–H/Å	H···A/Å	D–H···A/°
1	O–H1···N[a]	2.8080(12)	0.896(17)	1.972(17)	154.6(15)
2	O1–H1···N1[b]	2.7884(7)	0.98	1.86	157.8
	O2–H2···N2[c]	2.7796(6)	0.98	1.84	159.5

Symmetry codes: [a] = $-x, -y, 1-z$; [b] = $1-x, 2-y, -z$; [c] = $-x, 1-y, 1-z$.

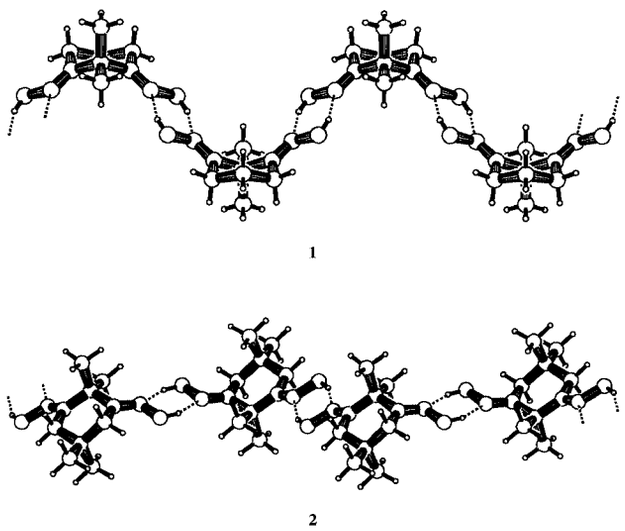

Fig. 3 Infinite, undulating polymer-like chains of **1** and **2** in the solid state shown as projections along the crystallographic directions [0 0 1] and [1 0 0], respectively. Dashed lines represent hydrogen bonds.

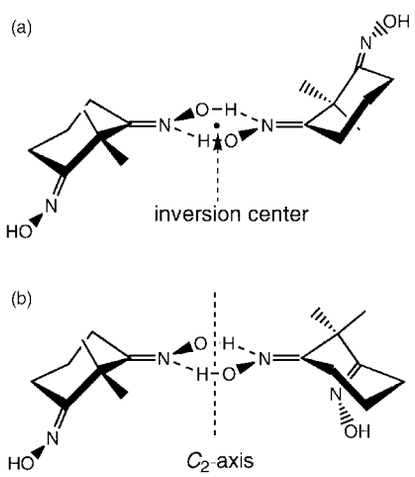

Fig. 4 Schematic representation of the two possible dimeric $R_2^2(6)$ hydrogen-bonding motifs for **1** and **2** with a) C_i-symmetry and b) C_2-symmetry.

distinct motifs which differ slightly in their structural features are found for **2** (Table 1). The O–N bond lengths as well as the C=N–O valence angles are in agreement with the average values of 1.408 Å and 112° found for hydrogen bonded oxime groups.[3] All hydrogen bond donor–acceptor (D···A) distances are significantly smaller than the sum of isotropic van der Waals radii for nitrogen and oxygen (N, 1.55 Å and O, 1.52 Å)[13] and the D···A distances are also shorter than the average N···O distance (2.822 Å) observed for other oxime dimers.[3] The D–H···A hydrogen bond angles (*ca.* 160°) are typical for moderate to strong hydrogen bonds.[14]

As a consequence of the intermolecular dimeric oxime hydrogen bonding in the solid state **1** and **2** assemble into infinite, one-dimensional polymer-like chains. These chains possess an undulating shape due to the 1,3-relationship of the two oxime functionalities (Fig. 3). Although this one-dimensional topology resembles that of 1,1′-bicyclohexylidene-4,4′-dione dioxime and its saturated analogue 1,1′-bicyclohexyl-4,4′-dione dioxime,[5d] the three-dimensional arrangement of the chains (packing motif) is markedly different. In the case of **1** and **2** all chains extend in a single crystallographic direction (**1**, [0 1 0] and **2**, [1 1 −1]) giving densely packed structures.[15] In contrast, the chains of 1,1-bicyclohexylidene-4,4′-dione dioxime and its saturated analogue are aligned parallel in layers. The chains occupying successive layers are oriented nearly perpendicularly with respect to each other.[5d]

In passing, it should be noted that the formation of the undulating chains of **1** and **2** is presumably controlled by the intermolecular dimeric oxime hydrogen-bonding motifs, which possess C_i-symmetry (Fig. 4a). Although not observed, the oxime moieties could also give $R_2^2(6)$ motifs with C_2- instead of C_i-symmetry (Fig. 4b). Had this been the case cyclic bracelet-like supramolecular assemblies consisting of *ca.* 10 molecules would have been obtained.[16] ‖

A charge density study of the intermolecular dimeric oxime hydrogen bonding $R_2^2(6)$ motif in 2

In principle all structural elements of an electronic system can be derived from the charge density distribution (CDD) $\rho(\boldsymbol{r})$ where $\boldsymbol{r}$ is a vector in crystal space.[9,17] ** Recently experimental determination of CDD's from high-resolution X-ray experiments has become feasible.[18] In these experiments the CDD's are represented by the 'rigid-pseudoatom' model, wherein the charge density deformations caused by interatomic interactions are described in terms of spherical harmonics multiplied by Slater-type radial functions with energy optimized exponents

‖ The number of molecules required for a cyclic assembly is estimated using the angle of *ca.* 135° between the two oxime groups in **1** or **2**. A similar interpretation was reported previously to rationalise the solid-state motifs of racemic and chiral 2,5-diazabicyclo[2.2.2]octane-3,6-dione.[16] For the racemic mixture, intermolecular dimeric amide hydrogen bonding [$R_2^2(6)$ motifs with C_i-symmetry] gave infinite polymer-like chains; chiral recognition between amide moieties with opposite configurations occurs. For the pure enantiomers cyclic hexamers [$R_2^2(6)$ motifs with C_2-symmetry] were expected. However, they were not observed.

** $\rho(\boldsymbol{r})$ is described in terms of critical points (CP) $\boldsymbol{r}_c$, at which the first derivative $\nabla\rho(\boldsymbol{r})$ vanishes. They are characterized by the second derivative or the number of non-zero eigenvalues λ of the curvature (Hessian) matrix and the sign s of the matrix (s = number of positive λs − number of negative λs). In a CDD four non-degenerate CP's with $\lambda = 3$ exist: maxima (3, −3), saddle points (3, −1) and (3, +1) and minima (3, +3) and their positions in crystal space obey the space group symmetry rules.[20] The bond ellipticity ε is defined as $\varepsilon = (\lambda_1/\lambda_2) - 1$. Whereas for σ type interactions $\varepsilon = 0$, ε concomitantly increases with increased π character. The presence of a (3, −1) CP on an interatomic interaction line (λ_1 and λ_2 perpendicular to this line are negative, while λ_3 in the direction of the line is positive) is regarded as an indication for bonding interaction. It represents the bond critical point (BCP) $\boldsymbol{r}_p$. Its position characterizes the polarity of the bond, *i.e.* $\boldsymbol{r}_p$ is shifted towards the less electronegative atom. The type of interaction is determined by the Laplacian at the BCP, *viz.* $\nabla^2\rho(\boldsymbol{r}_p) = \lambda_1 + \lambda_2 + \lambda_3$. It describes the *concentration* ($\nabla^2\rho(\boldsymbol{r}_p) < 0$) or *depletion* ($\nabla^2\rho(\boldsymbol{r}_p) > 0$) of charge density at $\boldsymbol{r}_p$ caused by the interatomic interaction. Since $\nabla^2\rho(\boldsymbol{r})$ has a finer structure than $\rho(\boldsymbol{r})$, it is more sensitive to small changes in CDD's. In general it is found that $\nabla^2\rho(\boldsymbol{r}_p) < 0$ for covalent bonds and $\nabla^2\rho(\boldsymbol{r}_p) > 0$ for closed shell interactions as in ionic, hydrogen bond and van der Waals complexes.

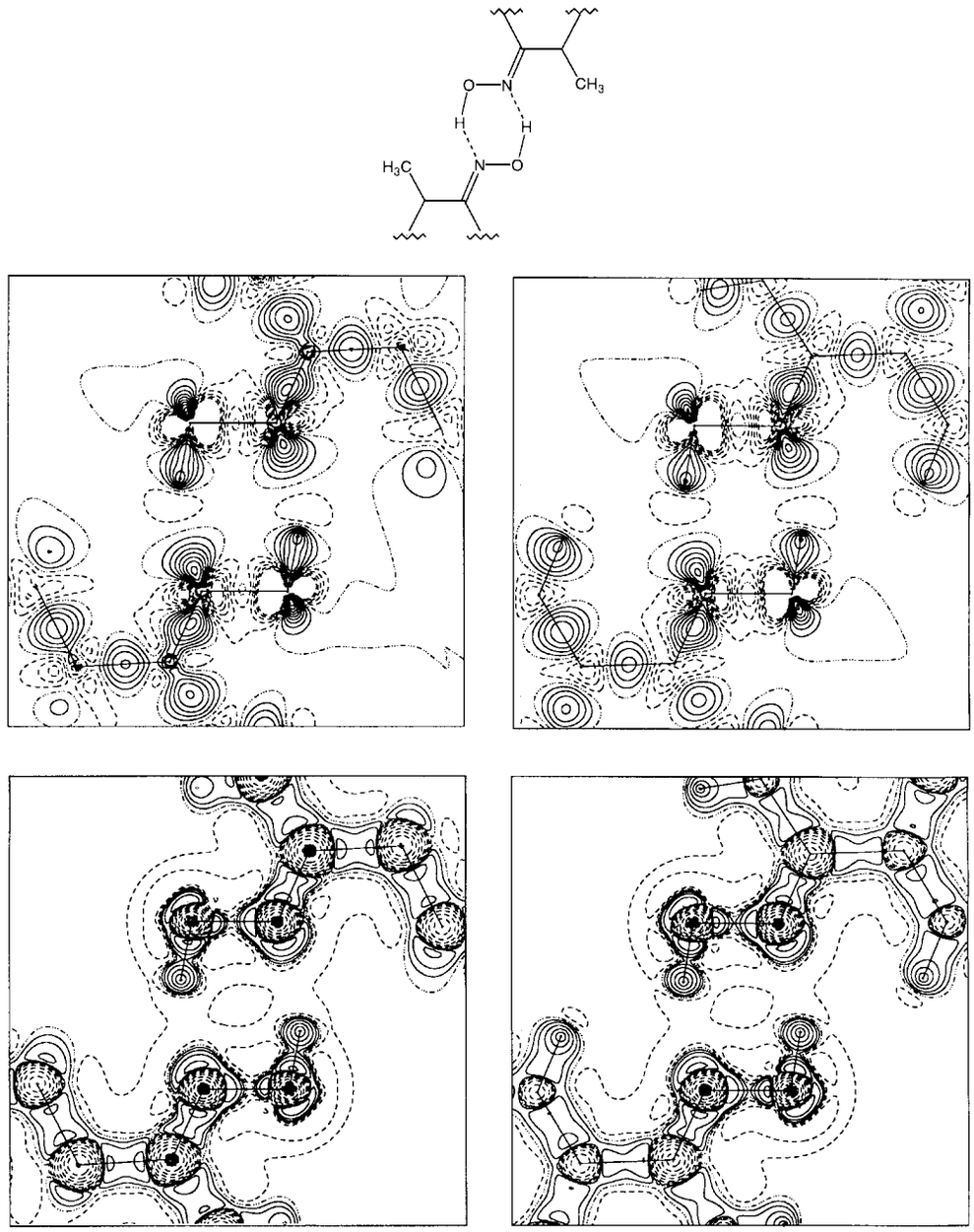

Fig. 5 Deformation density (top) and Laplacian of the electron density (bottom) in the plane of the two distinct oxime hydrogen bonding motifs of **2**. The motif of N1–O1–H1 is shown on the left, while that of N2–O2–H2 is depicted on the right. The contour levels of the deformation density and Laplacian are at 0.1 (e Å^{-3}) and e^n (e Å^{-5}) intervals, respectively. Negative contours are dashed.

up to a certain multipole expansion level.[19] In comparison with computational approaches, experimental CDD investigations pose fewer restrictions on the size of the system studied and more importantly, their results inherently reflect all interactions in the crystal.

To gain insight in the chemical bonding within the electronic system of the intermolecular dimeric oxime hydrogen-bonding motif [$R_2^2(6)$], the CDD of **2** was determined from its high resolution single crystal X-ray data and subjected to a Bader-type topological analysis.[9] This allows the defined partitioning of its chemical structure into sub-molecular regions (functional groups) by topological parameters such as the bond critical points (BCP's) $\boldsymbol{r}_p$ and their Laplacian values $\nabla^2\rho(\boldsymbol{r}_p)$.[20]

The experimental deformation densities and Laplacian maps of the CDD's of the two distinct oxime hydrogen bonding motifs of **2** reflect its molecular asymmetry (C_1, Fig. 5). Both the multipole populations as well as the BCP parameters substantiate this finding (Tables 2 and 3). All covalent bonds were successfully located by (3, −1) BCP's and have negative $\nabla^2\rho(\boldsymbol{r}_p)$ values. In contrast, the hydrogen bonds have positive $\nabla^2\rho(\boldsymbol{r}_p)$ values at their (3, −1) BCP's in line with their electrostatic nature. The positive values are in agreement with those previously found for related systems.[21] The positions of the BCP's reflect the polarities of the chemical bonds. For example, in the non-polar C–CH_3 bonds $\boldsymbol{r}_p$ is situated near the midpoint of the bond, whereas in the polar C=N bonds $\boldsymbol{r}_p$ is shifted towards the less electronegative atom. In the hydrogen bonds $\boldsymbol{r}_p$ is found near the hydrogen atom.

Whereas the results of the multipole analysis give an accurate description of the C–C and C–N bonds of **2**, the accurate description of the O–N bond turned out to be difficult (see Tables 2 and 3).[22] Initial experiments in which different models (octopolar expansion level for second row elements) and data sets were used resulted in positive values for $\nabla^2\rho(\boldsymbol{r}_p)$ of the O–N bonds! This is inconsistent with the covalent character of the O–N bond. Negative $\nabla^2\rho(\boldsymbol{r}_p)$ values were only obtained after introduction of hexadecapole parameters ($l = 4$) for second row elements as well as a constrained κ' for spherical valence shell expansion/contraction of the multipoles in the refinement. However, the magnitudes of these Laplacian $\nabla^2\rho(\boldsymbol{r}_p)$ values are

Table 2 Properties of the BCP's, r_p, in **2** (see Figs. 1 and 2 and Table 3)

Bond	$\rho(r_p)$/e Å^{-3}	$\nabla^2\rho(r_p)$/e Å^{-5}	λ_1/e Å^{-5}	λ_2/e Å^{-5}	λ_3/e Å^{-5}	ε
O1–N1	*1.976*	*−1.689*	*−17.00*	*−14.50*	*29.82*	*0.17*
O2–N2	*1.999*	*−4.489*	*−17.62*	*−16.66*	*29.79*	*0.06*
N1–C2	2.444	−19.943	−22.13	−18.62	20.81	0.19
N2–C6	2.421	−19.702	−22.31	−18.61	21.22	0.20
C1–C2	1.604	−14.357	−10.96	−10.39	6.99	0.06
C1–C6	1.620	−14.575	−11.18	−10.51	7.12	0.06
C1–C7	1.557	−13.295	−10.04	−9.97	6.71	0.01
C1–C8	1.670	−15.537	−11.42	−10.71	6.59	0.07
C2–C3	1.709	−15.192	−11.31	−10.62	6.74	0.06
C3–C4	1.574	−11.216	−10.40	−10.25	9.44	0.01
C4–C5	1.532	−11.579	−9.89	−9.88	8.19	0.00
C4–C9	1.611	−12.206	−11.29	−11.27	10.36	0.00
C4–C10	1.666	−13.336	−11.84	−11.59	10.10	0.02
C5–C6	1.702	−15.767	−11.42	−11.08	6.73	0.03
H1 · · · N1′[a]	0.207	3.398	−1.18	−1.07	5.65	0.10
H2 · · · N2″[a]	0.211	3.303	−1.24	−1.11	5.66	0.12

Symmetry codes: ′ = 1 − x, 2 − y, −z; ″ = −x, 1 − y, 1 − z. [a] The local kinetic energy density $G(r_p)$ for H1 · · · N1′ and H2 · · · N2″ and 0.774 and 0.765 e Å^{-5} resulting in $G(r_p)/\rho(r_p)$ ratios of 3.741 and 3.627 respectively.††

Table 3 Positions of the BCP's, r_p, in **2** (see Figs. 1 and 2)

Bond A–B	A–B/Å	A–r_p/Å	r_p–B/Å
O1–N1	1.4017	0.7256	0.6761
O2–N2	1.4108	0.7424	0.6685
N1–C2	1.2826	0.8509	0.4317
N2–C6	1.2838	0.8520	0.4318
C1–C2	1.5274	0.7372	0.7902
C1–C6	1.5319	0.7475	0.7844
C1–C7	1.5516	0.7617	0.7898
C1–C8	1.5336	0.7979	0.7357
C2–C3	1.5036	0.8205	0.6831
C3–C4	1.5396	0.7585	0.7812
C4–C5	1.5375	0.7373	0.8002
C4–C9	1.5326	0.7653	0.7674
C4–C10	1.5329	0.7471	0.7858
C5–C6	1.5053	0.7081	0.7972
N1′–H1	1.8735	1.2397	0.6338
N2″–H2	1.8575	1.2229	0.6346

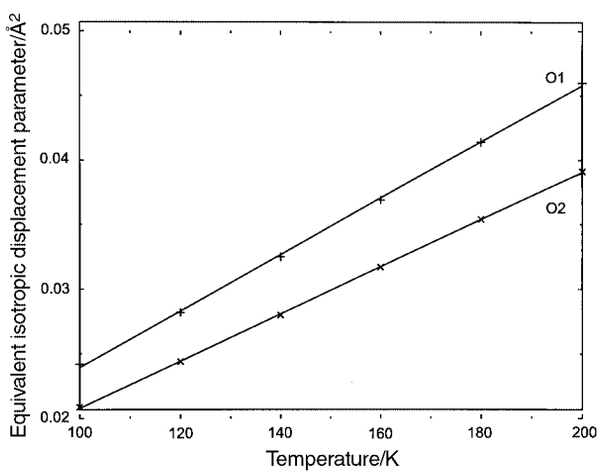

Fig. 6 Temperature dependent behaviour of the equivalent isotropic displacement parameters ($U_{eq} = \frac{1}{3}\sum_i\sum_j U_{ij}a^*_i a^*_j a_i a_j$) of O1 and O2 of **2**: $U_{eq}(O1) = 2.1(4) \times 10^{-3} + 2.19(3) \times 10^{-4}\ T$ and $U_{eq}(O2) = 2.5(1) \times 10^{-3} + 1.826(9) \times 10^{-4}\ T$.

still unexpectedly low (Table 2). It is of relevance that similar discrepancies were found for other covalent bonds between very electronegative atoms[23] like the O–N bonds in inorganic nitrites[24] and nitrates.[25]

To gain insight in the contributing factors to this anomaly, we have performed B3LYP/6-311++G** density functional calculations on acetone oxime followed by a Bader-type topological analysis (Table 4). The optimized geometry of acetone oxime was in agreement with its gas phase electron diffraction structure.[26] A comparison of the results reveals that for related C–C and C–N bonds the BCP's, $\rho(r_p)$, $\nabla^2\rho(r_p)$ as well as the bond ellipticity (ε) values are in excellent agreement (Tables 2, 3 and 4). This is, however, not the case for the O–N bonds. Whereas the related BCP's and $\rho(r_p)$ values are in line, substantial deviations are found for the $\nabla^2\rho(r_p)$ and ε values (**2**: O1–N1, $\nabla^2\rho(r_p)$ −1.689 e Å^{-5}, ε 0.17 and O2–N2, $\nabla^2\rho(r_p)$ −4.489 e Å^{-5}, ε 0.06 and acetone oxime: $\nabla^2\rho(r_p)$ −8.60 e Å^{-5}, ε 0.03)! Interestingly, the B3LYP/6-311++G** results of acetone oxime fully support the covalent character of the O–N bond and agree with chemical intuition. This suggests that the anomaly has to be attributed to the experimental values of λ_1, λ_2 and λ_3 of the two distinct O–N bonds in the case of **2**. Indeed in particular, deviations are observed between the values of λ_2 and λ_3 of **2** and acetone oxime, respectively (**2**: O1–N1, λ_1 −17.00, λ_2 −14.50 and λ_3 29.82 e Å^{-5} and O2–N2, λ_1 −17.62, λ_2 −16.66 and λ_3 29.79 e Å^{-5}, and acetone oxime: λ_1 −16.96, λ_2 −16.41 and λ_3 24.77 e Å^{-5}). Consequently, the bond ellipticity ε will be affected.[9] Hence, it has to be concluded that the CDD of the two distinct O–N bonds of **2** obtained by the multipole analysis is still not fully adequate.

The most important sources for the deviations of the topological parameters of the two O–N bonds are presumably the incomplete deconvolution of the atomic displacement parameters and the diffuse multipole parameters. The displacement ellipsoid plot of **2** shows that the anisotropic displacement of the nitrogen and oxygen atoms is mainly perpendicular to the bonds (Fig. 2). It therefore interferes with λ_1 and λ_2, which are also perpendicular to the bond. Detailed inspection of the displacement parameters reveals that, in fact, the displacement of O1 is larger than that of O2, reflecting the shorter intermolecular hydrogen bond of O2 (Table 1). This phenomenon was further evaluated by a temperature-dependent single-crystal X-ray structure analysis (see Experimental section). If the displacements are primarily generated by thermal

†† $G(r)$ can be interpreted as the action of the electronic charge at the BCP upon change of the hydrogen bond system, *i.e.* $G(r)$ decreases with a decreasing charge density $\rho(r)$ according to eqn. (1):

$$G(r) = \tfrac{3}{10}(3\pi^2)^{2/3}\rho(r)^{5/3} + \tfrac{1}{6}\nabla^2\rho(r) \quad (1)$$

An error of 5 to 15 kJ mol^{-1} for $G(r)$ and a maximum error of 0.02 Å for d(H · · · O) has to be taken into account. Hence, the derived values only provide a qualitative estimate.[28]

Table 4 Properties of the B3LYP/6-311++G** BCP's for acetone oxime

Bond A–B	A–B/Å [a]	A–r_p/Å	$\rho(r_p)$/e Å^{-3}	$\nabla^2\rho(r_p)$/e Å^{-5}	λ_1/e Å^{-5}	λ_2/e Å^{-5}	λ_3/e Å^{-5}	ε
O–N	*1.42* (*1.42*)	*0.77*	*1.96*	*−8.60*	*−16.96*	*−16.41*	*24.77*	*0.03*
N–C	1.28 (1.29)	0.83	2.47	−19.23	−21.91	−17.13	19.80	0.28
C_E–C	1.50 (1.50)	0.73	1.65	−14.78	−11.92	−11.35	8.50	0.05
C_Z–C	1.51 (1.50)	0.73	1.63	−14.34	−11.67	−11.20	8.53	0.04

[a] In parentheses, experimental values determined by gas phase diffraction, see ref. 26.

Table 5 IR and Raman frequencies (cm^{-1}) of oxime vibrations of **1** and **2** in the solid state (KBr). Solution (DMSO) data in parentheses

Compound	**1**		**2**	
Vibration	IR	Raman	IR	Raman
ν_{O-H}	3262	—[b]	3271	—[b]
δ_{O-H}	1470	1488	1484	1514
γ_{O-H}	760	—[b]	746	—[b]
$\nu_{C=N}$	1674 (1648)[a]	1660 (1650)	1670 (1652)	1663 (1653)
	1659 (1632)	1650 (1634)[a]	1651 (1633)	1645 (1635)

[a] Peak maximum determined from second derivative of spectrum (see Experimental section). [b] Not observed (see text).

vibrations they should reveal the forces acting on the particular atom or group.[27] Indeed, the results not only show that the displacement is larger for O1 than for O2 at 100 K, but that the temperature coefficient of the equivalent isotropic displacement (U_{eq}) is higher for O1. The linearity of the temperature dependency proves that the displacements are of thermal origin (Fig. 6). The stronger thermal vibration of O1 indicates that the topological parameters of the O1–N1 bond will be more biased which accounts for its deviant ε value (Table 2).

The topological parameters of the hydrogen bonds can be used to estimate the hydrogen bond strength by calculation of the local kinetic energy density $G(\boldsymbol{r})$ at the BCP.[21] For closed shell interactions such as hydrogen bonds, $G(\boldsymbol{r})$ can be directly derived from the experimental CDD's using Abramov's equation.[28]†† A statistical analysis showed that $G(\boldsymbol{r}_p)$ can be correlated to the H···O distance d(H···O) of hydrogen bonded O–H···O systems.[21] From our calculated $G(\boldsymbol{r})$ values of 0.774 and 0.765 e Å^{-5} (84.36 and 83.37 kJ mol^{-1} per atomic unit volume) hydrogen bond lengths d(H···N) of *ca.* 1.82 Å are found. The hydrogen bond dissociation energy is estimated to be 36 kJ mol^{-1} per atomic unit volume. Furthermore, the kinetic energy per electronic charge $G(\boldsymbol{r}_p)/\rho(\boldsymbol{r}_p)$ is greater than unity, *i.e.* the positive curvature λ_3 of $\rho(\boldsymbol{r}_p)$ is large and dominated by the contraction of charge towards the nuclei.

Solid-state and solution spectroscopy of 1 and 2

Since the intermolecular dimeric oxime hydrogen bonding are unequivocally defined, a detailed spectroscopic (^{13}C CP/MAS NMR, IR and Raman) analysis of this important $R_2^2(6)$ motif is feasible. The number of resonances in the solution ^{1}H and ^{13}C NMR spectra of **1** and **2** (see Experimental section) suggests that they possess average C_{2v}-symmetry on the NMR time-scale due to rapid interconversion of their conformers. In contrast, the solid-state ^{13}C CP/MAS NMR spectra of **1** and **2** are markedly different. For **1** a single broadened imine carbon resonance (δ 163.4 ppm, FWHM 64 Hz) is found, which after Gaussian enhancement gave an asymmetric doublet characteristic for the perturbation of the imine ^{13}C resonance by a quadrupole interaction of the ^{14}N nucleus.[29] In the case of **2** two distinct asymmetrical doublets (δ 161.5 ppm, FWHM 57 Hz and δ 165.4 ppm, FWHM 58 Hz) are discernible for the imine ^{13}C atoms. Furthermore, all methyl groups are anisochronous in the solid state (**1**: δ C2/2′ 22.4 and 25.7 ppm and **2**: δ C2/2′ 21.4, 25.9; C5/5′ 30.4, 32.3 ppm) and either one (**1**, δ 21.4 ppm) or two (**2**, δ 34.6 and 36.7 ppm) methylene resonances were found.[30,31] Hence, **1** possesses molecular C_S-symmetry, whereas **2** lacks symmetry (*vide supra*).

A comparison of the solid-state IR spectra of **1** or **2** with those of the corresponding O-deuterated derivatives (see Experimental section) allowed the unambiguous assignment of the O–H stretching (ν_{O-H}), the O–H *out-of-plane* (γ_{O-H}) and the O–H *in-plane* bending (δ_{O-H}) vibrations (Table 5). The solid-state IR spectra of **1** and **2** lack free O–H stretching vibrations, which appear in dilute CCl_4 solution at 3600 and 3605 cm^{-1}, respectively. Instead, broad composite bands consistent with the occurrence of moderately strong hydrogen bonding are observed,[15] which resemble those of the oligo(cyclohexylidene) mono- and dioximes.[5c,d]

The positions of γ_{O-H} (**1**, 760 and **2**, 746 cm^{-1}) are in agreement with those previously reported (*ca.* 760 cm^{-1}) and confirm that intermolecular dimeric oxime hydrogen bonding takes place.[5,32,33] ‡‡ Although the single crystal X-ray structure analysis and ^{13}C CP/MAS NMR show that **2** has two distinct $R_2^2(6)$ hydrogen bonding motifs, this is not immediately apparent from the IR and Raman data. However, differences between intermolecular hydrogen bonding motifs of **1** and **2** show up in the IR spectra upon cooling to −180 °C. The ν_{O-H} stretching bands of both **1** and **2** shift to lower wavenumbers. This is presumably due to strengthening of the hydrogen bonds; a considerably more complex band is observed for **2** than for **1** (Fig. 7). In contrast, the γ_{O-H} and δ_{O-H} vibrations of **1** and **2** shift to higher wavenumbers upon cooling. While at −180 °C for γ_{O-H} of **1** and **2** two (769 and 757 cm^{-1}) and three (767, 760 and 750 cm^{-1}) bands are found, respectively (Fig. 7), δ_{O-H} (**1**, 1470 and **2**, 1484 cm^{-1}), which is positioned near the CH_2 scissoring modes (1460–1440 cm^{-1}),[34] does not split upon cooling to −180 °C (**1**, 1480 and **2**, 1495 cm^{-1}). Unfortunately, the interpretation of the γ_{O-H} splitting pattern is hampered due to overlap with other peaks. Thus, despite the fact that the γ_{O-H} data show that intermolecular dimeric oxime hydrogen bonding occurs, it cannot be decided whether the $R_2^2(6)$ motifs possesses either local C_i- or C_2-symmetry. This issue can be resolved by a survey of δ_{O-H}, which is the only O–H vibration that is also discernible in the

‡‡ For trimeric oxime aggregates γ_{O-H} is positioned at *ca.* 800 cm^{-1}.[32,33]

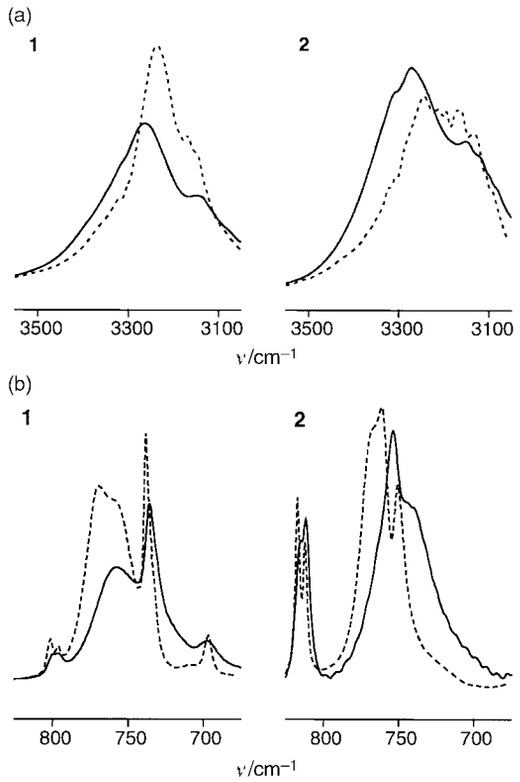

Fig. 7 Part of the solid state IR spectra of **1** and **2** showing their ν_{O-H} (a) and γ_{O-H} (b) at 20 °C (293 K, solid lines) and −180 °C (93 K, dashed lines).

Raman spectra of **1** and **2**. In the Raman spectra δ_{O-H} is positioned at higher wavenumbers than in the IR spectra indicating that *intermolecular* coupling of δ_{O-H} *via* the hydrogen-bonding $R_2^2(6)$ motif occurs. This coupling leads to a splitting of the δ_{O-H} vibrations into an *in-phase* and *out-of-phase* mode. Since mutual exclusion is observed, *i.e.* the *in-phase* vibration is only IR active while the *out-of-phase* is only Raman active, the $R_2^2(6)$ motifs have to possess local C_i-symmetry. This is further substantiated by the $\nu_{C=N}$ vibrational patterns. For **1** as well as **2** four peaks, of which two are IR- and two are Raman-active, are found at different wavenumbers (Fig. 8). These patterns can be rationalized using correlation field theory.[35] In analogy to the observed splitting of δ_{O-H}, *inter*molecular coupling of $\nu_{C=N}$ *via* the $R_2^2(6)$ motifs also results into an *in-phase* and *out-of-phase* mode. Each mode is further split into two novel ones due to an additional *intra*molecular coupling of $\nu_{C=N}$.[34] The occurrence of *intra*molecular coupling of $\nu_{C=N}$ is confirmed by solution IR and Raman (solvent, DMSO); for **1** as well as **2** a split band is positioned at identical frequencies.§§ As expected, the $\nu_{C=N}$ bands at lower wavenumber have the highest intensity in IR, whereas in Raman this order is reversed. A splitting of $\nu_{C=N}$ is not found in the solution IR and Raman spectra of the related *mono*-oxime 2,2-dimethylcyclohexanone oxime (**3**) and the average positions of the distinct $\nu_{C=N}$ bands of **1** or **2** nearly coincide with that of **3**.

Conclusions

Single crystal X-ray analyses show that in the solid state the (*E*,*E*)-stereoisomers **1** and **2** assemble into infinite, undulating polymer-like chains, due to centrosymmetric dimeric intermolecular oxime hydrogen bonding [$R_2^2(6)$ motifs]. Whereas **1** has molecular C_S-symmetry and shows skeletal disorder, **2** lacks symmetry. Notwithstanding the atomic positions of the oxime groups of **1** and **2** are unequivocally defined, *i.e.* oxime disorder is absent. The asymmetry of **2** is also reflected by the properties of the BCP's obtained by a topological analysis of the experimentally determined CCD's of **2**. For all located (3, −1) BCP's, except those of the hydrogen bonds, negative Laplacian $\nabla^2\rho(\boldsymbol{r}_p)$ values are found in line with the occurrence of covalent bonding. However, it is noteworthy that negative values for the Laplacians at the BCP's of the O–N bonds could only be obtained by refinement including hexadecapole parameters [$l = 4$] for the first row elements and constrained κ′ for spherical valence shell expansion/contraction of the multipoles. This anomaly was interpreted with the use of B3LYP/6-311++G** data on the model system acetone oxime. In line with expectation the hydrogen bonds O–H···N have positive values for the Laplacian at their BCP; the oxime hydrogen bonds are adequately described. The hydrogen bond dissociation energy was estimated to be 36 kJ mol^{-1} per atomic unit volume from a correlation of the local kinetic energy density and the hydrogen bond length.

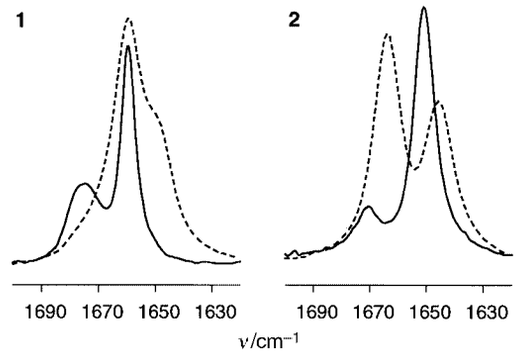

Fig. 8 Part of the solid-state IR (solid lines) and Raman (dashed lines) spectra of **1** and **2** showing the four distinct $\nu_{C=N}$ modes.

^{13}C CP/MAS NMR corroborate the molecular C_S-symmetry of **1** and the lack of symmetry of **2** in the solid state. The imino ^{13}C chemical shift is a sensitive probe to distinguish moderate changes in the structural features of the intermolecular dimeric oxime hydrogen bonding motifs. Vibrational analysis (IR) provides unequivocal evidence for the occurrence of dimeric oxime hydrogen bonding [$R_2^2(6)$ motifs]. The local symmetry (C_i) of these motifs can be established from the $\nu_{C=N}$ vibrational pattern in both IR and Raman. These results provide insight in the structural prerequisites required for the occurrence of well-defined intermolecular oxime hydrogen bonding, such as found in the $R_2^2(6)$ motifs of **1** and **2**. These motifs can be used as structural elements in the development of novel supramolecular assemblies.[5]

Experimental

General

Gas chromatography (GC): Varian 3350 gas chromatograph equipped with a capillary column (DB-5, 30 m × 0.323 mm, carrier gas H_2) and FID detection (temperature program: 100 (373 K)→280 °C (553 K), heating rate 20 °C min^{-1}). Solution NMR: Bruker AC 300 spectrometer (^{1}H, 300.13 MHz; ^{13}C, 75.47 MHz) using $CDCl_3$ as the solvent unless stated otherwise. TMS was used as internal reference. ^{1}H-^{1}H and ^{1}H-^{13}C shift correlation experiments (COSY) were performed using Bruker's standard pulse sequences. High-resolution ^{13}C CP/MAS NMR spectra were recorded at 22.5 °C (295.5 K) on a Varian ^{UNITY}INOVA spectrometer (^{13}C, 75.47 MHz) equipped with a 7 mm VT-CP/MAS probe. Samples were spun at 5 kHz in Si_3N_4 rotors and contained KBr (20%) for magic angle adjustment and *ca.* 5% hexamethylbenzene as an internal chemical shift reference (δ_C, 132.2 and 17.4 ppm).[36] Spin-lock cross-polarization and proton decoupling were achieved with rotating

§§ Preferential oxime–DMSO hydrogen bonding prevents intermolecular dimeric oxime hydrogen bonding.

magnetic field strengths of 44.8 and 39.3 kHz, respectively. Spectral editing of CH_3, CH_2, CH and C carbons by use of differences in their cross polarization properties was done by linear combination of three subspectra (CP, CPD, CPDR) with standard parameters.[30] Except for spectral editing experiments, total sideband suppression (TOSS) was used to eliminate spinning sidebands.[37] All aliphatic ^{13}C resonances were assigned using spectral editing techniques based on cross-polarization/repolarization methods. FT-IR spectra were recorded on a Perkin-Elmer system 2000 spectrometer equipped with either a low temperature sample unit for solids (KBr pellets) or with a liquid sample cell (NaCl windows, 0.5 mm path length). Solid-state temperature dependent IR measurements were performed from 20 °C (293 K) down to −180 °C (93 K). Oxygen deuterated derivatives of **1** and **2** were prepared by repeated dissolution in a dry acetone–$[^2H]CH_3OH$ mixture (v/v 1/1) followed by evaporation of the solvents *in vacuo*. Subsequently, the compounds were re-dissolved in a dry acetone–$[^2H]CH_3OH$ mixture (v/v 1/1) and crystallised from the solvent mixture. The isolated crystals were stored under a dry N_2 atmosphere. Raman spectra (resolution 4 cm^{-1}) were recorded with a Perkin-Elmer System 2000 spectrometer equipped with a Raman accessory. For neat polycrystalline samples a laser power of 1000 mW was used and 1024 scans were averaged. Solution Raman measurements were performed on saturated solutions of **1** and **2** in DMSO using laser powers of 700 and 1200 mW, respectively. To determine peak maxima deconvolution was performed using standard software. Melting points were determined in glass capillaries using a Mettler FP5 instrument (heating rate 3 °C min^{-1}). Thermogravimetric analysis (TGA) was done using a Perkin-Elmer TGS-2 apparatus equipped with an AR-2 autobalance (N_2, temperature program: 50 (323 K)→850 °C (1123 K), heating rate 5 °C min^{-1}). Wide angle X-ray powder diffraction (WAXD) patterns were measured at room temperature with 1.78897 Å Co radiation on an Enraf Nonius PDS120 X-ray Powder Diffractometry System equipped with a CPS120 curved gas flow detector with an argon–ethane gas purge operating in the self-quenching streamer mode of gas ionisation.

Syntheses

2,2-Dimethylcyclohexane-1,3-dione. This compound was prepared according to a modified literature procedure (scale 0.3 mol).[38,39] After the reaction mixture had been cooled to room temperature, ice (100 g) and conc. HCl (100 ml) were added. The resulting mixture was stirred for 30 min and extracted with diethyl ether (3 × 50 ml). Subsequent drying (Na_2SO_4) of the combined organic layers, followed by removal of the solvent *in vacuo* and Kugelrohr distillation (50–55 °C, 0.01 Torr) of the viscous residue gave pure product (28.3 g, 166 mmol, yield 52%), which had a purity of 95% (cap. GC). All spectral data were in agreement with those previously reported.[39]

2,2,5,5-Tetramethylcyclohexane-1,3-dione. This compound was prepared from commercially available dimedone (0.16 mol) following the procedure described for 2,2-dimethylcyclohexane-1,3-dione. After Kugelrohr distillation (65 °C, 0.01 Torr) the product (12.5 g, 63 mmol, yield 39%) was sufficiently pure (96%, cap. GC) for further use. The ^1H NMR spectrum of a sample obtained by re-crystallisation from hot C_2H_5OH was identical to that previously reported:[40] δ_C 22.16, 28.44, 30.62, 51.09, 60.36 and 210.38; ν_{max}(KBr)/cm^{-1} 1689 and 1725 (C=O).

(*E*,*E*)-2,2-Dimethylcyclohexane-1,3-dione dioxime (1) and (*E*,*E*)-2,2,5,5-tetramethylcyclohexane-1,3-dione dioxime (2). A mixture of the parent diketone (21.4 mmol), $H_2NOH{\cdot}HCl$ (3.12 g, 44.9 mmol), $NaHCO_3$ (4.5 g, 53.5 mmol) and C_2H_5OH (50 ml) was heated at reflux temperature for 24 h. After cooling to room temperature and addition of CH_2Cl_2 (50 ml), the mixture was filtered and the solid residue washed with C_2H_5OH–CH_2Cl_2 (v/v 1/1, 50 ml). The combined organic phases were subsequently dried (Na_2SO_4) and filtered, after which removal of solvent *in vacuo* afforded the crude product in quantitative yield. Recrystallisation from acetone gave the pure products. **1**: mp 200 °C (decomp.); $T_{subl.}$ 150 °C (TGA); δ_H ($[^2H_6]$DMSO) 1.29, 1.62, 2.53 and 10.53; δ_C($[2H_6]$DMSO) 22.52, 23.56, 28.35, 45.70 and 163.44; ν_{max}(KBr)/cm^{-1} 757 (O–H), 939 (O–N), 1659 and 1674 (C=N), 3262 (O–H); ν_{max}(DMSO)/cm^{-1} 1632 and 1648 (C=N); Raman ν_{max}(neat solid)/cm^{-1} 1514 (O–H), 1650 and 1660 (C=N); Raman ν_{max}(DMSO)/cm^{-1} 1634 and 1650 (C=N); WAXD d = 6.54, 6.21, 5.94, 5.52, 5.10, 4.70, 4.29, 4.03, 3.88, 3.48, 3.28, 3.12, 3.02, 2.57, 2.54 and 2.28. **2**: mp 238 °C (decomp.); T_{subl} 150 °C (TGA); δ_H($[^2H_6]$DMSO) 0.85 (s, 6H, CH_3), 1.25 (s, 6H, 2 × CH_3), 2.46 (s, 4H, 2 × CH_2) and 10.45 (s, 2H, 2 × OH); δ_C($[^2H_6]$DMSO) 27.47, 30.34, 35.12, 35.90, 45.66 and 162.83; CP/MAS NMR: δ_C 21.34, 25.85, 30.37, 32.21, 32.60, 34.49, 36.58, 43.81, 161.54 and 165.42; ν_{max}(KBr)/cm^{-1} 746 (O–H), 932 (O–N), 1484 (O–H), 1650 and 1670 (C=N), 3271 (O–H); ν_{max}(DMSO)/cm^{-1} 1633 and 1652 (C=N); Raman ν_{max}(neat solid)/cm^{-1} 1514 (O–H), 1645 and 1663 (C=N); Raman ν_{max}(DMSO)/cm^{-1} 1635 and 1653 (C=N); WAXD: d = 7.21, 6.73, 6.06, 5.30, 5.18, 4.42, 3.81, 3.76, 3.48, 3.44, 3.40, 3.38, 3.04 and 2.72.

Cyclohexane-1,3-dione dioxime and 5,5-dimethylcyclohexane-1,3-dione dioxime. Both compounds were obtained as a mixture of three stereoisomers using the procedures for **1** and **2** (Scheme 1). Cyclohexane-1,3-dione dioxime: ^1H NMR ($[^2H_6]$DMSO) was in agreement with that previously reported;[11] ratio (*E*,*E*):(*Z*,*E*)/(*E*,*Z*):(*Z*,*Z*) 1:1.4:1; 5,5-Dimethylcyclohexane-1,3-dione dioxime: δ_H($[^2H_6]$DMSO) (*E*,*E*) 0.88 (s, 6H, 2 × CH_3), 2.38 (s, 4H, 2 × CH_2), 2.87 (s, 2H, CH_2), 10.32 (s, 2H, 2 × OH); (*Z*,*E*)/(*E*,*Z*) 0.87 (s, 6H, 2 × CH_3), 2.11 (s, 2H, CH_2), 2.38 (s, 2H, CH_2), 3.16 (s, 2H, CH_2), 10.36 (s, 1H, OH), 10.39 (s, 1H, OH); (*Z*,*Z*) 0.86 (s, 6H, 2 × CH_3), 2.14 (s, 4H, 2 × CH_2) 3.40 (s, 3H, CH_3) and 10.42 (s, 2H, 2 × OH); δ_C($[^2H_6]$DMSO) (*Z*,*E*)/(*E*,*Z*) 30.18, 32.09, 34.66, 39.50, 46.42, 155.64 and 155.79; (*Z*,*Z*) 25.61, 29.84, 34.14, 46.31 and 155.08; (*E*,*E*) 30.39, 34.95, 39.19, 39.50 and 156.27; ratio (*E*,*E*):(*Z*,*E*)/(*E*,*Z*):(*Z*,*Z*) 4.5:4.5:1; All assignments were made by ^1H-^1H and ^1H-^{13}C COSY experiments.

2,2-Dimethylcyclohexanone oxime (3). 2,2-Dimethylcyclohexanone[41] (1.0 g, 8 mmol) was converted into **3** as described for **1**. After cooling the reaction mixture to room temperature, water (50 ml) was added and the reaction mixture was extracted with $CHCl_3$ (2 × 25 ml). The combined organic phases were dried (Na_2SO_4), filtered and evaporated *in vacuo* giving the crude product (0.8 g, 5.66 mmol, yield 71%). Pure **3** was obtained after sublimation (50 °C, 0.1–0.08 Torr): mp 94.4 °C (lit.,[42] 92–93 °C). Its ^1H NMR spectral data were identical with those previously reported;[43] δ_C 20.72, 21.71, 26.05, 26.55, 37.56, 41.23 and 165.49; ν_{max}(KBr)/cm^{-1} 776 (O–H), 935 (O–N), 1666 (C=N), 3233 (O–H); Raman ν_{max}(neat solid)/cm^{-1} 1655 (C=N); ν_{max}(DMSO)/cm^{-1} 1641 (C=N); Raman ν_{max}(DMSO)/cm^{-1} 1642 (C=N).

X-Ray structure determinations

Single crystal X-ray structure determination of 1.¶¶ Diffractometer: Nonius Kappa CCD with rotating anode (λ = 0.71073 Å). Colourless block 0.50 × 0.25 × 0.15 mm^3. $C_8H_{14}N_2O_2$, M_r = 170.21 g mol^{-1}, orthorhombic, *Pnma*, a = 10.0872(2), b = 11.7970(2), c = 7.7925(2) Å, V = 927.30(3) $Å^3$, Z = 4, ρ_{calcd} = 1.219 g cm^{-3}, T = 150(2) K, $(\sin\theta\lambda^{-1})_{max}$ = 0.649 $Å^{-1}$, measured reflections: 8793, unique reflections: 1114 (R_{int} = 0.0404). No absorption correction was considered necessary.

¶¶ CCDC reference number 188/212. See http://www.rsc.org/suppdata/p2/a9/a900335i for crystallographic files in .cif format.

Structure solution with direct methods (SHELXS-97).[44] Structure refinement with SHELXL-97 against F^2 of all data.[45] R-values ($I > 2\sigma(I)$): $R1 = 0.0360$, $wR2 = 0.0963$; all data: $R1 = 0.0428$, $wR2 = 0.1018$, $S = 1.062$, $-0.16 < \Delta\rho < 0.27$ e Å^{-3}.

Single crystal X-ray structure determination of 2.¶¶ Diffractometer: Nonius Kappa CCD with rotating anode ($\lambda = 0.71073$ Å). Colourless block $0.31 \times 0.31 \times 0.31$ mm^3. $C_{10}H_{18}N_2O_2$, $M_r = 198.26$, triclinic, $P\bar{1}$, $a = 7.1363(2)$, $b = 7.2813(2)$, $c = 11.6544(3)$ Å, $\alpha = 87.8805(18)$, $\beta = 72.1948(13)$, $\gamma = 82.7986(16)°$, $V = 572.03(3)$ Å^3, $Z = 2$, $\rho_{calcd} = 1.151$ g cm^{-3}, $T = 100(2)$ K, $(\sin\theta\lambda^{-1})_{max} = 1.080$ Å^{-1}, measured reflections: 67635, unique reflections: 11896 ($R_{int} = 0.049$). Evaluation of the intensities with the DENZO-SMN package.[46] Analytical absorption correction ($\mu = 0.08$ mm^{-1}, 0.96–0.98 transmission) with PLATON, routine ABST.[47] Data merged with the SORTAV package.[48] Structure solution with direct methods (SHELXS-97).[44] Structure refinement with the XD package against F using all 7332 observed reflections with $I > 3\sigma(I)$.[49] Multipole parameters for C, N and O atoms were refined up to $l = 4$ and for H atoms up to $l = 1$. Multipole parameters refining to a value $x \leq |0.01|$ were set to 0 and fixed. Hydrogen atoms were normalised to distances derived from neutron data (O–H: 0.98 Å, C–H: 1.08 Å). Positional and displacement parameters of H atoms were not refined. One constraint was included in the refinement for keeping the charge of the molecule neutral and additional constraints for keeping the κ'_l the same for all l. Differences of mean-square displacement amplitudes $\Delta_{A,B}$ are smaller than 0.001 Å^2 for all bonds. R-values ($I > 3\sigma(I)$): $R1 = 0.0221$, all data: $R1 = 0.0442$. $-0.15 < \Delta\rho < 0.20$ e Å^{-3}.

Temperature dependent single crystal X-ray structure analysis of 2. A colourless crystal of **2** ($0.15 \times 0.30 \times 0.42$ mm^3) was mounted on a Nonius Kappa CCD diffractometer with rotating anode ($\lambda = 0.71073$ Å). Subsequently, six complete data sets were measured at temperatures of 100, 120, 140, 160, 180 and 200 K. The data sets were integrated with the DENZO-SMN package.[46] The unit cell parameters showed linear behaviour with respect to the temperature: $a = 7.1013(12) + 2.51(8) \times 10^{-4}\ T$, $b = 7.2545(5) + 1.68(3) \times 10^{-4}\ T$, $c = 11.560(11) + 7.87(7) \times 10^{-4}\ T$, $\alpha = 88.21(9) - 3.26(6) \times 10^{-3}\ T$, $\beta = 72.61(6) - 4.32(4) \times 10^{-3}\ T$, $\gamma = 82.94(3) - 1.25(2) \times 10^{-3}\ T$ (temperature in K, axes in Å and angles in °). The relationship between thermal parameters and hydrogen bond strength has been found before in careful neutron studies of water molecules.[50] The reflections were checked for higher Laue symmetry with PLATON.[47] Refinement was done with SHELXL-97[45] against F^2 of all data up to a resolution of $(\sin\theta\lambda^{-1})_{max} = 0.65$ Å^{-1}. Non-hydrogen atoms were refined freely with anisotropic parameters. C–H hydrogen atoms were refined as rigid groups and O–H hydrogen atoms were refined freely with isotropic parameters. The resulting R-values were in the range $R1$ (obs. refl.): 0.0361 (100 K)–0.0424 (200 K).

Ab Initio calculations on acetone oxime

The geometry of acetone oxime (C_S-symmetry) was optimized at the B3LYP/6-311++G** level of theory using the Gamess-UK[51] program. A topological Bader analysis[52] was carried out using the Gaussian 98[53] package.

Acknowledgements

Contributions by Dr J. H. van Lenthe (Theoretical Chemistry Group, Utrecht University) concerning the Bader type analysis of acetone oxime as well as financial support in part (M. L., A. L. S.) by the Council for Chemical Sciences of the Netherlands Organization for Scientific Research (CW-NWO) are gratefully acknowledged.

References

1 J.-M. Lehn, *Supramolecular Chemistry*, VCH, Weinheim, 1995; G. R. Desiraju, *The Crystal as a Supramolecular Entity*, Wiley, 1996.
2 M. C. Etter, *J. Phys. Chem.*, 1991, **95**, 4601; E. Fan, C. Vicent, S. J. Geib and A. D. Hamilton, *Chem. Mater.*, 1994, **6**, 1113; J. C. MacDonald and G. M. Whitesides, *Chem. Rev.*, 1994, **94**, 2383; See also the special issue on molecular networks; *New J. Chem.*, 1998, 87.
3 V. Bertolasi, G. Gilli and A. C. Veronese, *Acta Crystallogr.*, *Sect. B*, 1982, **38**, 502; L. Chertanova, C. Pascard and A. Sheremetev, *Acta Crystallogr.*, *Sect. B*, 1994, **50**, 708.
4 F. J. Hoogesteger, R. W. A. Havenith, J. W. Zwikker, L. W. Jenneskens, H. Kooijman, N. Veldman and A. L. Spek, *J. Org. Chem.*, 1995, **60**, 4375.
5 (*a*) F. J. Hoogesteger, J. M. Kroon, L. W. Jenneskens, E. J. R. Sudhölter, T. J. M. de Bruin, J. W. Zwikker, E. ten Grotenhuis, C. H. M. Mareé, N. Veldman and A. L. Spek, *Langmuir*, 1996, **12**, 4760; (*b*) E. ten Grotenhuis, A.W. Marsman, F. J. Hoogesteger, J. C. van Miltenburg, J. P. van der Eerden, L. W. Jenneskens, W. J. J. Smeets and A. L. Spek, *J. Cryst. Growth*, 1998, **191**, 834 and references cited; (*c*) F. J. Hoogesteger, L. W. Jenneskens, H. Kooijman, N. Veldman and A. L. Spek, *Tetrahedron*, 1996, **52**, 1773; (*d*) A. W. Marsman, E. D. Leusink, J. W. Zwikker, L. W. Jenneskens, W. J. J. Smeets, N. Veldman and A. L. Spek, *Chem. Mater.*, 1999, **11**, 1484.
6 C. B. Aakeröy, A. M Beatty and D. S. Leinen, *J. Am. Chem. Soc.*, 1998, **120**, 7383.
7 M. Raban, D. Kost, W. B. Jennings and V. E. Wilson, in *Acyclic Organonitrogen Stereodynamics*, eds. J. B. Lambert and Y. Takeuchi, VCH, Weinheim, 1991, pp. 57–88 and 177–193.
8 M. E. Jung, P. A. Blair and J. A. Lowe, *Tetrahedron Lett.*, 1976, **18**, 1439 and references cited therein.
9 R. F. W. Bader, *Atoms in Molecules*: *A Quantum Theory*, Clarendon Press, Oxford, 1990.
10 J. March, *Advanced Organic Chemistry*, 3rd edn., Wiley, New York, 1985, p. 805.
11 H. Saitô and K. Nukada, *Tetrahedron Lett.*, 1965, **25**, 2117.
12 A. Kotali, V. P. Papageorgiou and P. G. Tsoungas, *Org. Mass. Spectrom.*, 1987, **22**, 373.
13 A. J. Bondi, *J. Phys. Chem.*, 1964, **68**, 441.
14 G. A. Jeffrey, *An Introduction to Hydrogen Bonding*, Oxford University Press, New York, 1997.
15 A. I. Kitaigorodski, *Molecular Crystals and Molecules*, Academic Press, New York, 1973.
16 M.-J. Brienne, J. Gabard, M. Leclerq, J.-M. Lehn, M. Cesario, C. Pascard, M. Chevé and G. Dutruc-Rosset, *Tetrahedron Lett.*, 1994, **35**, 8157.
17 R. F. W. Bader, P. Lode, A. Popelier and T. A. Keith, *Angew. Chem.*, *Int. Ed. Eng.*, 1994, **106**, 620.
18 T. Koritsánszky, R. Flaig, D. Zobel, H.-G. Krane, W. Morgenroth and P. Luger, *Science*, 1998, **279**, 356; R. Flaig, T. Koritsánszky, J. Janczak, H.-G. Krane, W. Morgenroth and P. Luger, *Angew. Chem.*, *Int. Ed. Engl.*, 1999, **38**, 1397.
19 N. K. Hansen and P. Coppens, *Acta Crystallogr.*, *Sect. A*, 1978, **34**, 909.
20 V. Tsirelson, Y. Abramov, V. Zavodnik, A. Stash, E. Belokoneva, J. Stahn, U. Pietsch and D. Feil, *Struct. Chem.*, 1998, **9**, 249 and references cited therein; M. Souhassou and R.H. Blessing, *J. Appl. Crystallogr.*, 1999, **32**, 210.
21 E. Espinosa, E. Molins and C. Lecomte, *Chem. Phys. Lett.*, 1998, **285**, 170.
22 See also R. Glaser and A. Streitwieser, *J. Am. Chem. Soc.*, 1989, **111**, 7340.
23 D. Cremer and E. Kraka, *Croat. Chem. Acta*, 1984, **57**, 1259.
24 S. Ohba, K. Toriumi, S. Sato and Y. Saito, *Acta Crystallogr.*, *Sect. B*, 1978, **34**, 3535.
25 G. de With, S. Harkema and D. Feil, *Acta Crystallogr.*, *Sect. A*, 1975, **31**, S227.
26 K. Iijima, M. Suzuki, T. Sakaizumi and O. Ohashi, *J. Mol. Struct.*, 1997, **413–414**, 327.
27 J. D. Dunitz, V. Schomaker and K. N. Trueblood, *J. Phys. Chem.*, 1988, **92**, 856.
28 Y. A. Abramov, *Acta Crystallogr.*, *Sect. A*, 1997, **53**, 264.
29 M. C. Etter, S. M. Reutzel and G. M. Vojta, *J. Mol. Struct.*, 1990, **237**, 165; A. Naito, S. Ganapathy and C. A. McDowell, *J. Magn. Reson.*, 1982, **48**, 367.
30 R. Sangill, N. Rastrup-Andersen, H. Bildsøe, H. J. Jakobsen and N. C. Nielsen, *J. Magn. Reson. A*, 1994, **107**, 67.
31 H. Paulsen, K. Todt and H. Rippenberger, *Chem. Ber.*, 1968, **101**, 3365; F. J. Hoogesteger, D. M. Grove, L. W. Jenneskens, T. J. M. de Bruin and B. A. J. Jansen, *J. Chem. Soc.*, *Perkin Trans. 2*, 1996, 2327.

32 See also Y. Okaya, A. Shimada and I. Nitta, *Bull. Chem. Soc. Jpn.*, 1956, **29**, 210; T. K. Bierlein and E. C. Lingafelter, *Acta Crystallogr.*, 1951, **4**, 450.
33 (*a*) H. Saitô, K. Nukada and M. Ohno, *Tetrahedron Lett.*, 1964, **31**, 2124 and references cited therein; (*b*) W. C. Harris and S. F. Bush, *J. Chem. Phys.*, 1972, **56**, 6147 and references cited therein.
34 D. Lin-Vien, N. B. Colthup, W. G. Fateley and J. G. Grasselli, *The Handbook of Infrared and Raman Characteristic Frequencies of Organic Molecules*, Academic Press, San Diego, 1991, ch. 9.
35 F. A. Cotton, *Chemical Applications of Group Theory*, 3rd edn., Wiley, New York, 1990, pp. 338–347.
36 W. L. Earl and D. L. Vanderhart, *J. Magn. Reson.*, 1982, **48**, 35.
37 W. T. Dixon, *J. Magn. Reson.*, 1981, **44**, 220.
38 B. M. Jacobson, P. Soleropoulos and S. Bahadori, *J. Org. Chem.*, 1988, **53**, 3247.
39 K. Mori and H. Mori, *Org. Synth.*, 1990, **68**, 56.
40 T. W. Theobald, *Tetrahedron*, 1978, **34**, 1567.
41 F. E. King, T. J. King and J. G. Topliss, *J. Chem. Soc.*, 1957, 919.
42 S. Horvat, P. Karallas and J. M. White, *J. Chem. Soc.*, *Perkin Trans. 2*, 1998, 2151.
43 G. Just and L. S. Ng, *Can. J. Chem.*, 1968, **46**, 3381.
44 G. M. Sheldrick, *SHELXS-97, Program for Crystal Structure Solution*, University of Göttingen, Germany, 1997.
45 G. M. Sheldrick, *SHELXL-97, Program for Crystal Structure Refinement*, University of Göttingen, Germany, 1997.
46 Z. Otwinowski and W. Minor, *Methods Enzymol.*, vol. 276: *Macromolecular Crystallography*, part A, eds. C. W. Carter, Jr. and R. M. Sweets, Academic Press, 1997, 307.
47 A. L. Spek, *A Multipurpose Crystallographic Tool*, Utrecht University, The Netherlands 1998.
48 R. H. Blessing, *J. Appl. Crystallogr.*, 1997, **30**, 421.
49 T. Koritsánszky, S. Howard, P. R. Mallison, Z. Su, T. Richter and N. K. Hansen, *A Computer Program Package for Multipole Refinement and Analysis of Electron Densities form Diffraction Data*, Free University of Berlin, Germany, 1995.
50 A. Eriksson and K. Hermansson, *Acta Crystallogr., Sect. B*, 1983, **39**, 703.
51 GAMESS-UK is package of *ab initio* programs written by: M. F. Guest, J. H. van Lenthe, J. Kendrick, K. Schoffel, P. Sherwood and R. J. Harrison with contributions from: R. D. Amos, R. J. Buenker, M. Dupuis, N. C. Handy, I. H. Miller, P. J. Knowles, V. Bonacic-Koutecky, W. von Niessen, V. R. Saunders and A. J. Stone. The package is derived from the original GAMESS code due to M. Dupuis, D. Spangler and J. Wendolowski, *NRCC Software Catalog*, 1980, vol. 1, Program No. QG01 (GAMESS).
52 J. Cioslowski and B. B. Stefanov, *Mol. Phys.*, 1995, **84**, 707.
53 Gaussian 98, Revision A.6, M. J. Frisch, G. W. Trucks, H. B. Schlegel, G. E. Scusera, M. A. Robb, J. R. Cheeseman, V. G. Zakrzewski, J. A. Montgomery, Jr., R. E. Stratmann, J. C. Burant, S. Dapprich, J. M. Millam, A. D. Daniels, K. N. Kudin, M. C. Strain, O. Farkas, J. Tomasi, V. Barone, M. Cossi, R. Cammi, B. Mennucci, C. Pomelli, C. Adamo, S. Clifford, J. Ochterski, G. A. Petersson, P. Y. Ayala, Q. Cui, K. Morokuma, D. K. Malick, A. D. Rabuck, K. Raghavachari, J. B. Foresman, J. Cioslowski, J. V. Ortiz, B. B. Stefanov, G. Liu, A. Liashenko, P. Piskorz, I. Komaromi, R. Gomperts, R. L. Martin, D. J. Fox, T. Keith, M. A. Al-Laham, C. Y. Peng, A. Nanayakkara, C. Gonzalez, M. Head-Gordon, E. S. Replogle and J. A. Pople, Gaussian, Inc., Pittsburg, PA, 1998.

Paper a908335i